特集　14
研究解説

Accurate Schemes for the Numerical Simulation of Incompressible Flows

非圧縮性流れ数値解析のための高精度スキーム

Ayodeji O. DEMUREN*, Robert V. WILSON**, Mark CARPENTER*** and Toshio KOBAYASHI*
アヨデジ　オー　デムレン・ロバート　ヴィ　ウィルソン・マーク　カーペンター・小　林　敏　雄

Accurate numerical schemes are proposed for solving incompressible Navier-Stokes equations for 2D or 3D fluid flow problems. These are based on low-storage Runge-Kutta schemes for temporal discretization and fourth and sixth order compact schemes for spatial discretization. The incompressibility requirement is satisfied by solving a Poisson equation for pressure, with the same compact scheme used for discretization to ensure consistent global accuracy. The accuracy of the present procedure is demonstrated by application to several pertinent benchmark problems.

1. INTRODUCTION

For direct numerical simulation (DNS) of fluid flow problems, it is generally accepted that higher-order accurate methods must be used to minimize dissipation and dispersion errors. As the flow Reynolds number increases so do the ranges of temporal and spatial scales which must be resolved. Thus, the number of grid points-per-wavelength (PPW) required by the numerical scheme for approximation of the flow equations to within acceptable tolerances of dissipation and dispersion errors effectively limits the smallest scales that can be computed accurately, and thereby also the maximum Reynolds number. Spectral methods require the fewest PPW, namely two, and are therefore ideal for computations of flows with periodic boundary conditions. For more general flow problems finite-difference methods are desirable. Lele [1] has analyzed the resolution qualities of several finite-difference schemes. In general, resolution increased, i.e., fewer PPW, the larger the computational grid stencil, and implicit compact schemes had better resolution than regular explicit schemes of the same order of accuracy and computational stencil. Further, high resolution properties could be improved by optimization of coefficients, but at the expense of the formal order of accuracy. Haras and Ta'asan [2] suggested that schemes should be optimized for global accuracy rather than resolution efficiency. Hu et al. [3] have also shown that, in applications of interest to computational acoustics, temporal resolution could be improved by optimization of the coefficients of any multi-stage, Runge-Kutta, time-advancing approximation scheme.

In large eddy simulation (LES) of turbulent flows, the goal is not to resolve all the scales in the flow, but only the larger scales. Effects of the unresolved smaller scales are approximated with sub-grid scale (SGS) models. Therefore, second-order, central-difference schemes are often used [4, 5]. A further justification is that effects of truncation errors may be comparable to uncertainties inherent in the SGS models. However, questions remain as to how large the "larger" scales are, and how many PPW are required to resolve the smallest scale in the range. It is obvious that if LES is to be used in computational acoustics, dispersion errors are unacceptable [6]. Dynamic SGS models also presume accurate resolution of the flow on the grid and test scales. Higher-order-accurate (greater than second-order) methods guarantee much better convergence towards grid independence, along with better wave-number resolution. In addition, implicit (compact) finite-difference schemes require narrower computational grid stencils, have better fine-scale resolution and yield better global accuracy than explicit finite-difference schemes with the same formal order of accuracy. Therefore, the present

*Center for Collaborative Research, University of Tokyo
**Department of Mechanical Engineering, Old Dominion University
***Acoustic and Flow Methods Branch, NASA Langley Research Center

study focuses on the use of higher-order (fourth and sixth) compact schemes for the simulation of incompressible fluid flow problems.

The lack of an evolution equation for the pressure presents particular difficulty in the computation of incompressible flows, which is absent in compressible flows. An auxiliary equation has to be derived for the pressure which is then solved to satisfy the divergence-free velocity-field condition required for incompressibility. In the present study, the Poisson equation for pressure will be discretized with the same compact finite-difference scheme as used in the Navier-Stokes equations. Extension to irregular grids in physical space simply requires transformation of the equations onto a regular grid in computational space. The metrics of the transformation must be computed with the same compact finite-difference scheme to guarantee a consistent level of accuracy. Further details can be found in Wilson et al. [7].

2. ANALYSIS

2.1 Governing Differential Equations

The partial differential equations governing the incompressible fluid flow are the Navier-Stokes equations which can be written in Cartesian tensor form, for dimensionless variables as:

$$\frac{\partial u_i}{\partial t}+u_j\frac{\partial u_i}{\partial x_j}=-\frac{\partial p}{\partial x_i}+\frac{1}{\mathrm{Re}_D}\frac{\partial^2 u_i}{\partial x_j\partial x_j} \quad \cdots\cdots (1)$$

where, u_i are the Cartesian velocity components in the Cartesian coordinate directions x_i, p is the pressure and Re_D is the Reynolds number based on the equivalent diameter D_e. These equations must be solved in conjuction with the continuity equation:

$$\frac{\partial u_i}{\partial x_i}=0 \quad \cdots\cdots (2)$$

which expresses the divergence-free velocity condition. In 2D, i or j = 1, 2 and in 3D, i or j = 1, 2, 3. Einstein's summation rule for repeated indices is presumed.

2.2 Discretization

The Navier-Stokes equations (1) are discretized temporally with explicit Runge-Kutta (RK) schemes, and spatially with implicit compact finite difference schemes. The discretized equation has the form:

$$u_i^{n+1}=u_i^n+b^M\Delta t\left[H_i^M-\delta_{x_i}P^M\right] \quad \cdots\cdots (3)$$

with

$$H_i^M=-u_j\delta_{xj}u_i^M+\frac{1}{\mathrm{Re}_{D_e}}\delta_{xxj}u_i^M$$

i.e., the sum of convection and diffusion (CD) terms.

In Eq. (3), n represents the time step and M stands for the M_{th} stage of the RK scheme, with the corresponding coefficient b^M. δ_{xj} and δ_{xxj} are compact first and second derivative operators, respectively.

The momentum equation is advanced from time level, n, to n + 1, using Q substages. The temporal derivative in the momentum equation is discretized using a third- or fourth-order explicit RK scheme:

$$\frac{\delta u_i}{\delta t}\approx\frac{u_i^{M+1}-u_i^M}{b^M\Delta t}=H_i^M-\frac{\partial p^M}{\partial x_i}=\hat{H}_i^M \quad \cdots\cdots (4)$$

where u_i^M represents the x_i velocity component at the M_{th} substage (M = 0 is equivalent to the n_{th} time level, $M = Q$ to the n + 1_{th} time level).

Low-storage is accomplished by continuously overwriting the storage location for the time derivatives and unknown variables at each sub-stage:

$$\hat{H}_i^M\leftarrow a^M\hat{H}_i^{M-1} \quad \cdots\cdots (5)$$

$$u_i^{M+1}\leftarrow u_i^M+b^M\Delta t\hat{H}_i^M \quad \cdots\cdots (6)$$

Table 1 gives values of the coefficients, a^M and b^M for some low-storage, 3-stage-third-order [8] and 5-stage-fourth-order [9] schemes.

The first derivative terms which appear in the governing equations are approximated using fourth- and sixth-order compact finite difference schemes described by Lele [1]. Higher accuracy derives from the implicit treatment of derivatives, via:

$$\alpha\phi'_{i-1}+\phi'_i+\alpha\phi'_{i+1}=\frac{a}{2\Delta x}\left(\phi_{i+1}-\phi_{i-1}\right)+\frac{b}{4\Delta x}\left(\phi_{i+2}-\phi_{i-2}\right) \quad \cdots (7)$$

(or in matrix form: $A_x\phi' = B_x\phi$ or $\phi' = A_x^{-1}B_x\phi$), where $\Delta x = L_x/(N_x\text{-}1)$, N_x is the number of grid points, ϕ'_i represents the first derivative of the generic variable ϕ_i with respect to x,

Table 1　Coefficients of the Runge-Kutta schemes.

	3-stage, 3rd-order		5-stage, 4th-order	
M	a^M	b^M	a^M	b^M
1	0	0.500	0	0.14965902
2	-0.68301270	0.91068360	-0.41789047	0.37921031
3	-1.33333333	0.36602540	-1.19215169	0.82295502
4			-1.69778469	0.69945045
5			-1.51418344	0.15305724

and α, a, b are the coefficients of the compact scheme which determine the accuracy. Similar expressions are used for derivatives with respect to the y and z directions. For the fourth-order scheme:,$\alpha = 1/4$, $a = 3/2$, and $b = 0$, and for the sixth-order scheme: $\alpha = 1/3$, $a = 14/9$, and $b = 1/9$. The LHS of Eq. (7) contains the unknown derivatives at grid points i and $i + 1$ while the RHS contains the known functional values ϕ_i at the grid points i $\pm$ 1 and i $\pm$ 2. A_x is a tridiagonal $N_x \times N_x$ matrix and B_x is a tridiagonal matrix for the fourth-order scheme and pentadiagonal matrix for the sixth-order scheme.

Similarly, second derivatives , which are present in the viscous terms of the momentum equation and the Laplacian operator of the Poisson equation for pressure are approximated using fourth- and sixth-order compact finite differences:

$$\alpha\phi''_{i-1} + \phi''_i + \alpha\phi''_{i+1} = \frac{a}{(\Delta x)^2}\left(\phi_{i+1} - 2\phi_i + \phi_{i-1}\right) + \frac{b}{4(\Delta x)^2}\left(\phi_{i+2} - 2\phi_i + \phi_{i-2}\right) \quad \cdots\cdots\cdots\cdots (8)$$

(or in matrix form: $A_{xx}\phi'' = B_{xx}\phi$ or $\phi'' = A_{xx}^{-1}B_{xx}\phi$). For the fourth-order scheme: $\alpha = 1/10$, $a = 6/5$, and $b = 0$, and for the sixth-order scheme: $\alpha = 2/11$, $a = 12/11$, and $b = 3/11$. A comparison of the leading truncation errors of explicit central difference and implicit compact approximations is given in Table 2. We see reductions by a factor of 4 for the fourth-order scheme and 9 for the sixth-order scheme in comparison to explicit central difference schemes of the same order, and corresponding reductions by factors of 2 and 4 for the first and second derivative approximations, respectively.

Equations (7) and (8) , written at all grid points, give tridiagonal systems of algebraic equations that can be solved efficiently by factoring the LHS into lower/upper (LU) systems once at the beginning of the simulation. Since the LU factors are geometric functions which do not change with the flow, they can be reused when derivatives are required. Special boundary schemes are required at non-periodic boundaries [1, 7].

2.3 The Continuity Equation and the Poisson Equation

Table 2　Comparison of the leading truncation errors of explicit and implicit central difference approximations.

Scheme	First derivative	Second derivative
fourth-order central	$(-4/5!)(\Delta x_j)^4\phi^{(5)}$	$(-8/6!)(\Delta x_j)^4\phi^{(6)}$
fourth-order compact	$(-1/5!)(\Delta x_j)^4\phi^{(5)}$	$(-3.6/6!)(\Delta x_j)^4\phi^{(6)}$
sixth-order central	$(-36/7!)(\Delta x_j)^6\phi^{(7)}$	$(-72/8!)(\Delta x_j)^6\phi^{(8)}$
sixth-order compact	$(-4/7!)(\Delta x_j)^6\phi^{(7)}$	$(-16.7/8!)(\Delta x_j)^6\phi^{(8)}$

for Pressure

Application of the divergence operator δ_{xi} to the discretized momentum equation (4) gives:

$$\frac{1}{b^M\Delta t}\left\{\delta_{xi}\left(u_i^{M+1} - u_i^M\right)\right\} = \delta_{xi}H_i^M - \delta_{xi}\delta_{xi}P^M \quad \cdots\cdots\cdots (9)$$

The term, $\delta_{xi}u_i^{M+1}$, represents the discretized continuity equation at the M + 1 sub-stage and is set to zero to enforce the divergence-free condition. The term, $\delta_{xi}u_i^M$, represents the divergence of the velocity field at the previous substage M. In practice, this term is retained to "kill off" any accumulation from previous substages due to lack of convergence, etc. The term, $\delta_{xi}H_i^M$, is the source term of the Poisson equation and represents gradients of the convection and diffusion terms which are known from the previous sub-stage. The term, $\delta_{xi}\delta_{xi}P^M$, represents the discretized Laplacian operator on the pressure.

The Last term in Eq. (9) represents a discretized Laplacian operator composed of two applications of the first derivative operator, δ_{xi}. It is well known that using two first derivative operators to represent the Laplacian operator on non-staggered grids can lead to an "odd-even" decoupling of the solution. To alleviate this problem, the Laplacian operator is discretized using a single second derivative operator:

$$\delta_{xx_i}P^M = \delta_{x_i}\left[H_i^M + \frac{u_i^M}{b^M\Delta t}\right] \quad \cdots\cdots\cdots\cdots\cdots\cdots (10)$$

where $\delta_{xxi}P^M$ represents the discrete Laplacian of pressure which is discretized with the compact second derivative operator given by Eq. (8).

Equation (10) can be written in the form of a system of equations as:

$$AP = \left[A_{xx}^{-1}B_{xx} + A_{yy}^{-1}B_{yy}\right]P = F \quad \cdots\cdots\cdots\cdots\cdots (11)$$

Equation (11) results in a "cross" type stencil at the i, j node in which all points along lines passing through the central node contribute to the stencil. For uniform grids, we can use the commutative property of the A matrices to derive:

$$\left[A_{yy}B_{xx} + A_{xx}B_{yy}\right]P = A_{yy}A_{xx}F \quad \cdots\cdots\cdots\cdots\cdots (12)$$

which has a "grid" type stencil that is more compact and much cheaper to solve. See Wilson et al. [7] for details.

Equation (11) or (12) must be solved to convergence at every substage of every time step, to ensure a divergence-free velocity field. Without this, the order of accuracy of the RK scheme can-

not be assured. Although the matrices are sparse, direct (sparse) methods of solution were found to be competitive only for fairly coarse-grid 2D problems. Multigrid iterative methods were by far the most efficient for large systems; in comparison to ADI, conjugate-gradient, GMRES, etc.

3. RESULTS AND DISCUSSION

The performance of the numerical formulation is tested, along with those of some popular schemes, by application to a variety of benchmark problems.

3.1 1-D Convection of a Gaussian

The first problem to be solved is the 1-D convection of a Gaussian profile:

$$\frac{\partial u}{\partial t} + c\frac{\partial u}{\partial x} = 0 \quad \cdots\cdots (13)$$

$$subject\ to: u(x,0) = 0.5\exp\left[-\left(\frac{x}{3}\right)^2 \ln(2)\right];$$

$$-20 \le x \le 450; \Delta x = 1, c = 1$$

This could test the time advancement scheme and the numerical approximation to the first derivative. Three spatial schemes are used. The exact solution corresponds to the convection of the initial profile at the constant wave speed, c. The third-order RK scheme was used to advance the equation in time for all spatial schemes. In addition, the CFL number was kept small so that resulting errors are due solely to the spatial formulation. Figure 1 shows computed solutions at t = 400 after the profile has convected to x = 400. There is little discernible difference between the exact solution and the solution with the fourth-order compact scheme. However, the solutions with the second-order central difference and the third-order upwind approximations show greatly reduced peak values and large, dispersive waves trailing the Gaussian profile. The errors from the second-order central difference scheme are the most severe. Distortion in the shape of the profile indicates dissipation and/or dispersion errors in the solution.

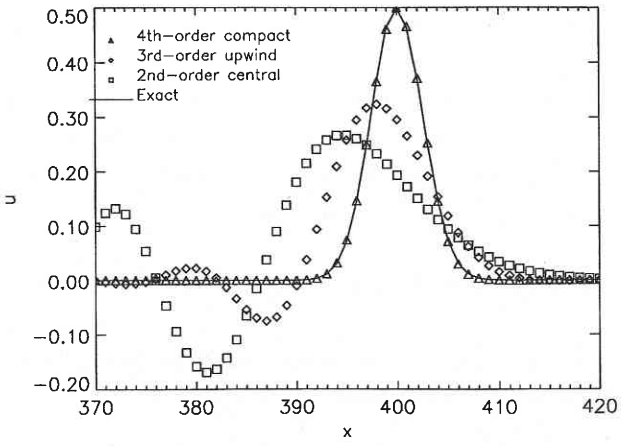

Fig. 1　Solution to the 1-D convection equation at t = in physical space for various finite difference approximations of the first derivative term.

To differentiate between dispersive and dissipative errors the solutions are transformed into wavenumber space using a Fourier transform method and compared with the exact solution in Fig. 2. The graph displays the resulting complex Fourier coefficient in polar form with the amplitude displayed in Fig. 2a and the phase angle in Fig. 2b. These show that both the second-order central difference and fourth-order compact schemes predict the correct amplitude for all modes, and hence are not dissipative. On the other hand, the amplitude of the solution computed with the third-order upwind scheme is reduced or dissipated, especially at higher wavenumbers. Figure 2b shows that only the fourth-order compact scheme predicts the correct phase angle for all wave-numbers. The phase angle from the second- and third-order solutions are only correctly predicted for the very lowest wavenumbers (k < *0.2* for the second-order solution, and k < *0.3* for the third-order solution). Large dispersion errors are evident at high wavenumbers.

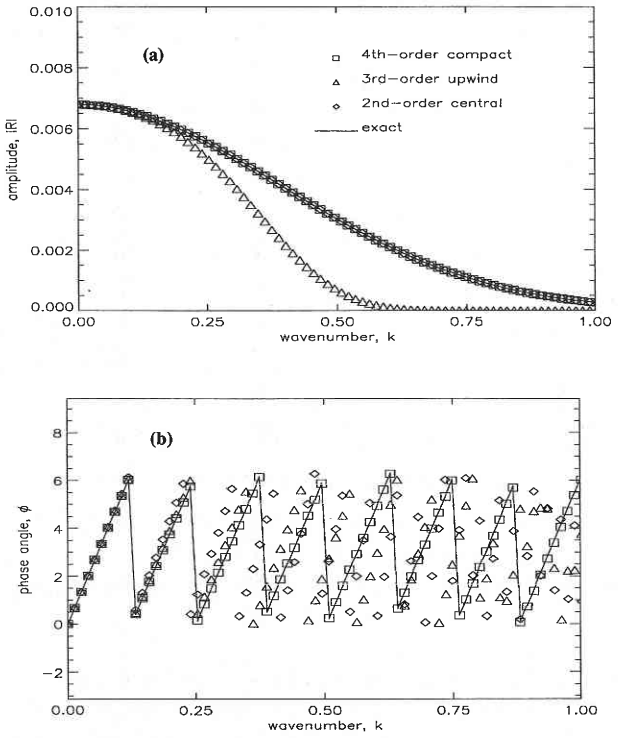

Fig. 2　Solution to the 1-D convection equation at t = 400 in wavenumber space for various finite difference approximations of the first derivative term, (a) amplitude and (b) phase angle.

3.2 1-D Convection of a Spherical Wave

The second problem is the solution of the 1-D convection equation in a spherical coordinate system. The governing equation takes the form:

$$\frac{\partial u}{\partial t}+\frac{u}{x}+\frac{\partial u}{\partial x}=0 \quad \cdots\cdots (14)$$

$$subject\ to: u(x,0)=0; u(5,t)=\sin\left(\frac{\pi t}{4}\right);$$

$$5\le x\le 450; \Delta x=1$$

The exact solution is a damped sine wave due to the presence of the u/x term in the governing equation when it is expressed in Cartesian coordinates. Fig. 3 compares exact and computed results at t = 400, for the region, 200 < x < 220. The upwind solution with 8 PPW shows severely reduced amplitude and a phase shift relative to the exact solution. Even those with 16 PPW and 32 PPW are not very accurate. It takes roughly 64 PPW (not shown) to reproduce the exact solution with the third-order upwind scheme, whereas the fourth-order compact scheme is able to reproduce the exact solution with 8 PPW.

3.3 2-D Convection Equation

Multidimensional effects of the numerical formulation are explored by solving the problem of the convection of an inverted cone around a circle. This problem is governed by the 2-D convection equation:

$$\frac{\partial u}{\partial t}+c_x\frac{\partial u}{\partial x}+c_y\frac{\partial u}{\partial y}=0 \quad \cdots\cdots (15)$$

where c_x = -y and c_y = x, are the convection speeds in the x and y directions, respectively. The initial conditions are that of an inverted sharp cone centered at x, y = -0.5, 0. The exact solution corresponds to the cone being convected counterclockwise in a circular path of radius, r_o = 0.5 with a period of 2π. Distortion of the shape of the cone is an indication of dispersion and/or dissipation errors.

Figure 4 shows computed results after one revolution of the cone using (*a*) third-order upwind approximation and (*b*) fourth-order compact approximation to the first derivatives on a 32 x 32 grid with uniform spacing. This grid defines the shape of the cone with a maximum of 8 points in each coordinate direction. The exact shape of the cone is included to the right of the computed solution at x, y = 0.5, 0 for comparison purposes. The

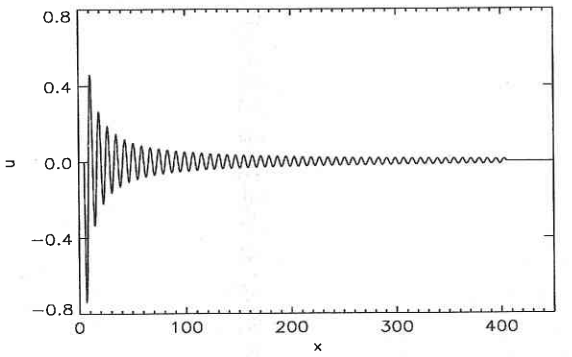

Fig. 3 a　Exact solution to the spherical wave problem at t = 400.

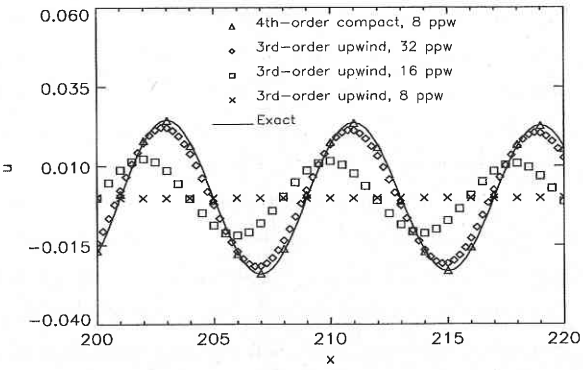

Fig. 3 b　Numerical solution of the 1-D spherical wave problem at t = 400 for the region, 200 < x < 220.

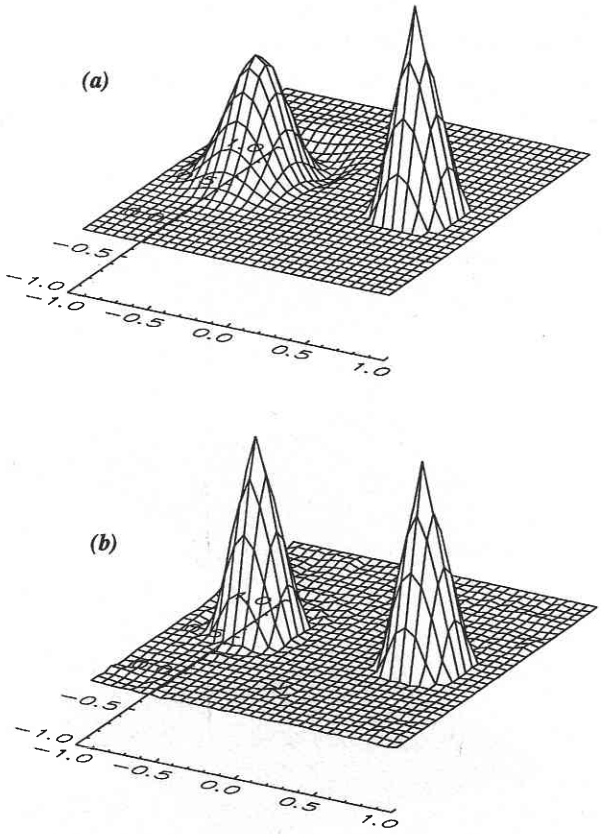

Fig 4　Numerical solution of the roating cone problem after one revolution on a 32 x 32 grid (a) third-order upwind scheme, (b) fourth-order compact scheme. Numerical solution is shown to the left, exact solution to the right.

third-order solution (Fig 4a) shows that the sharp point of the cone is greatly diffused and that dispersion errors are evident trailing the cone. A grid of 128 x 128 (or 32 points defining the shape of the cone) must be used with the third-order upwind approximation before the shape of the cone is faithfully reproduced. The fourth-order compact solution (Fig 4b) shows that the shape of the cone is not distorted as it is convected around the circle on the 32 x 32 grid. Indeed, the only noticeable error is a very small "grid to grid" oscillation. Figure 5 shows results for the same problem after one revolution, obtained by Orszag [10] using (*a*) second-order Arakawa finite-difference, (*b*) fourth-order Arakawa finite-difference, and (*c*) spectral schemes on a 32 x 32 grid. The finite difference solutions show errors similar to the third-order solutions in Fig. 4. The spectral method, which provides exact differentiation for all wavenumbers representable on the 32 x 32 grid, convects the cone without distortion, but some background waviness is also seen. The higher accuracy and resolution characteristics are achieved by the implicit treatment of derivatives. Even though the stencil size of the compact scheme is finite, implicit treatment of derivatives makes the scheme global, much like spectral methods.

3.4 Euler/Navier-Stokes Equations

In previous sections, the effect of numerical approximation on the accuracy of the convection terms was documented. In this section, the accuracy of the enforcement of the continuity equation through the solution of the Poisson equation for pressure is documented by solving the 2-D Euler/Navier-Stokes equations. Since the Navier-Stokes equations contain viscous terms, the numerical approximation to the second derivative is also tested. The test problems chosen for validation contain many features of the 3-D jets which are simulated in the current study. In this respect, the test problems are not merely academic exercises. The benchmark problems solved are; (*i*) a temporally-developing plane mixing layer (2-D Stuart's problem), and (*ii*) 2-D viscous wave decay.

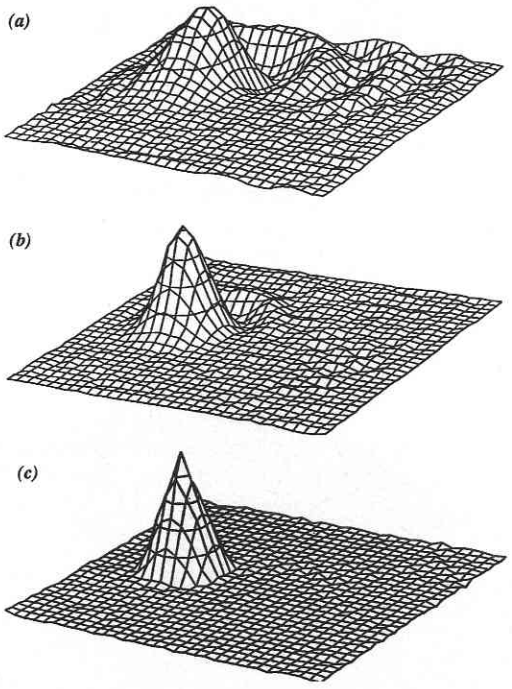

Fig 5　Numerical solution of the rotating cone problem after one revolution on a 32 x 32 grid from Orszag [10], (a) second-order Arakawa scheme, (b) fourth-order Arakawa scheme, and (c) spectral methods.

3.4.1 Temporally-Developing Plane Mixing Layer

An exact solution for the temporally-developing mixing layer was first published by Stuart [11], for the case with a disturbance of neutral mode. The initial conditions for the 2-D Stuart's problem correspond to a steady hyperbolic tangent function for the streamwise velocity component with a periodic array of vortex cores in the mixing region which cause the solution to vary in time. The wavelength of the disturbance corresponds to the neutral mode such that the disturbance is convected in the streamwise direction with no change in amplitude. The exact solution for the streamwise and transverse velocity components, u and v is given by:

$$u(x,y,t) = c + \frac{C\ \sinh(y)}{C\ \cosh(y) + A\ \cos(x-ct)}$$

$$v(x,y,t) = c + \frac{A\ \sin(x-ct)}{C\ \cosh(y) + A\ \cos(x-ct)} \cdots\cdots\cdots (16)$$

where $A = \sqrt{C^2-1}$ is a parameter which controls the strength of the perturbation and c is the convective speed of the mixing layer. The flow is periodic in the streamwise direction with length, $L_x = 2\pi$, $0 \le x \le 2\pi$. The flow is infinite in the transverse direction but in this study is truncated at a finite distance, $-L_y \le y \le L_y$, such that the zero-traction freestream boundary condition is applicable. Tests show that $L_y = 10$ is sufficiently large. Computed and exact solutions are compared in Fig. 6a with parameters, $c = 1$, $A = 1/2$. A uniform, cartesian grid is used for the simulations in this section. Unless otherwise specified, the third-order RK scheme is used for time advancement and time steps are sufficiently small so that spatial errors are dominant.

Figure 6b shows the numerical solution at $t = 20\pi$ (ten flow through times) on a relatively coarse grid of 13 (streamwise) x 41 (transverse) using the fourth-order compact approximation of convection terms and pressure. Even though the grid is relatively coarse (13 streamwise points per wavelength and roughly 8 points in the mixing region at $y \sim 0$) , there is little discernible

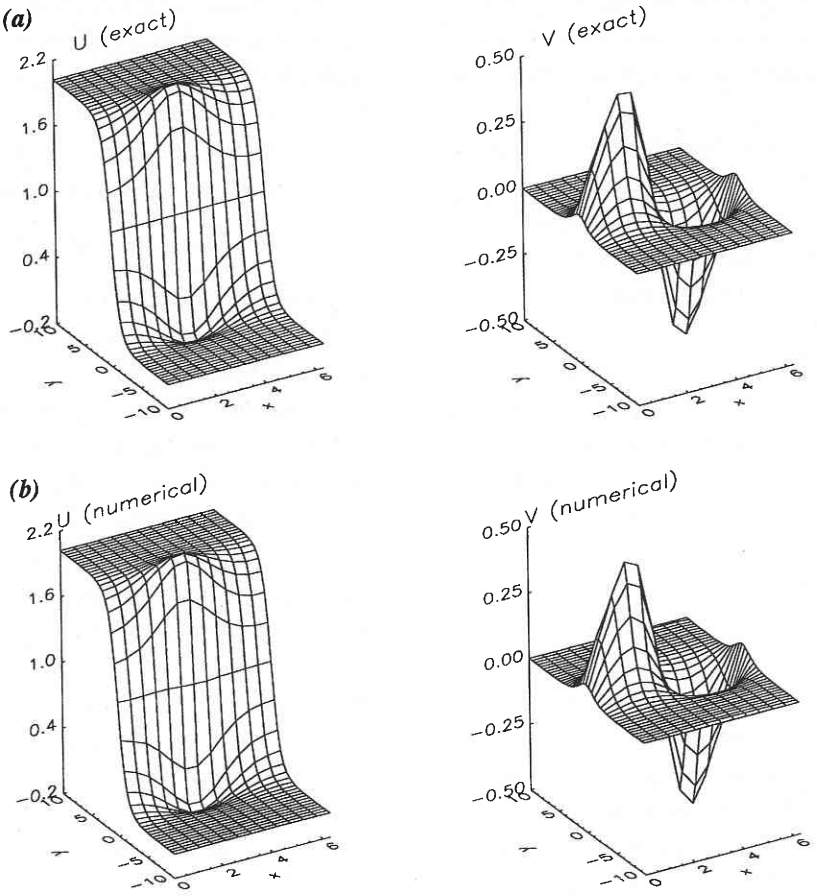

Fig 6 Solution of the Stuart's problem, (a) Exact solution and (b) numerical solution using fourth-order compact scheme on a 13 x 41 grid at t = 20π.

difference between the exact and numerical solutions after ten flow through times. Grid convergence rates are confirmed in terms of L2-norms of the error in u and v in Table 4. The order, N, is computed using the solution error from three grids of spacing, h, $2h$, and $4h$:

$$N = \frac{\ln\left[\dfrac{\phi_h - \phi_{2h}}{\phi_{2h} - \phi_{4h}}\right]}{\ln 2} \quad \cdots\cdots (17)$$

where ϕ_h, ϕ_{2h}, ϕ_{4h} are the errors on the h, $2h$,and $4h$ grids, respectively. Equation (17) assumes that the leading truncation error term is dominant (Demuren and Wilson [12]).

To address the effect of computing the pressure with a lower-order formulation, the 2-D Stuart's problem was solved using second-order central, fourth-order compact and sixth-order compact approximations of the convection terms but a second-order central difference solution of the pressure. These results, presented in Table 5, show that the lower-order solution of pressure results in the overall convergence of the error being second-order, even if the convection terms receive a higher-order treatment. All terms must be discretized using higher-order approximations to achieve higher-order error convergence rates. Thus, formulations presented in the literature, such as by Najjar

Table 4 Solution errors for 2-D Stuart's problem at t = 0.1.

	Fourth-order compact		Sixth-order compact	
Grid (ni x ni)	L2 Norm U	L2 Norm V	L2 Norm U	L2 Norm V
13 x 41	0.18×10^{-3}	0.24×10^{-3}	0.97×10^{-4}	0.11×10^{-3}
25 x 81	0.80×10^{-5}	0.11×10^{-4}	0.12×10^{-5}	0.14×10^{-5}
49 x 161	0.57×10^{-6}	0.74×10^{-6}	0.25×10^{-6}	0.45×10^{-6}
Order (N)	4.5	4.5	6.3	6.2

Table 5 Errors with different discretization of convection, but second-order for pressure.

	Second-order central		Fourth-order compact		Sixth-order compact	
Grid (ni x ni)	L2 Norm U	L2 Norm V	L2 Norm U	L2 Norm V	L2 Norm U	L2 Norm V
13 x 41	0.21×10^{-2}	0.20×10^{-2}	0.20×10^{-2}	0.20×10^{-2}	0.20×10^{-2}	0.20×10^{-2}
25 x 81	0.45×10^{-3}	0.53×10^{-3}	0.42×10^{-3}	0.44×10^{-3}	0.42×10^{-3}	0.44×10^{-3}
49 x 161	0.11×10^{-3}	0.13×10^{-3}	0.11×10^{-3}	0.11×10^{-3}	0.10×10^{-3}	0.11×10^{-3}
Order (N)	2.3	2.1	2.4	2.2	2.3	2.2

and Tafti [13], which use higher-order differences for the convection and diffusion terms but second-order differences for the Poisson equation for pressure would only be globally second-order accurate.

Temporal accuracy of the overall RK schemes is confirmed by performing computations for the 2-D Stuart's problem on the 49 by 161 grid with three different time steps. The results are shown in Table 6. The velocity field is specified from the exact solution and the vorticity is computed as a passive scalar.

3.4.2 Viscous Wave Decay

The numerical treatment of viscous terms is validated by solving the 2-D viscous wave decay problem which is governed by the Navier-Stokes equations. The domain for this problem is periodic in both the x and y directions where periodic boundary conditions are applied. The exact solution is given by:

$$u(x,y,t) = -\cos(x)\sin(y)\,e^{-\left(\frac{2t}{\mathrm{Re}}\right)}$$

$$v(x,y,t) = \sin(x)\cos(y)\,e^{-\left(\frac{2t}{\mathrm{Re}}\right)}$$

where Re = 20, $L_x = L_y = 1$. The exact solution consists of sinusoidal waves in the x and y directions which decay in time. Table 7 shows the L2 norm of the error at t = 0.025 using the fourth- and sixth-order compact approximations for convection and diffusion terms and the solution of pressure. The results are compared to the fourth-order, Essentially Non-Oscillatory (ENO) scheme from Weinan and Shu [14]. The error converges at fourth- and sixth-order rates thus validating the numerical treatment of the viscous terms and again validating the convection terms and the solution of pressure. The error of the ENO scheme converges at a fourth-order rate, but is more than two orders of magnitude greater than the fourth-order compact results. The error magnitude of the sixth-order compact formulation on the 128 x 128 grid has reached the round-off error level ($\sim 10^{-13}$) of the Cray supercomputer, indicating that extremely accurate results are obtained on average-sized grids.

Table 6 Solution errors for 2-D Stuart's Problem at t = 1.0, with different RK schemes.

		3-3 RK scheme	5-4 RK scheme
Grid (ni x ni)	Time Step	L2 Norm of Vorticity Error	L2 Norm of Vorticity Error
49 x 161	0.05	0.12803×10^{-4}	0.69910×10^{-6}
49 x 161	0.025	0.17157×10^{-5}	0.63575×10^{-6}
49 x 161	0.0125	0.66280×10^{-6}	0.63328×10^{-6}
Order (N)		3.4	4.7

Table 7 Solution errors for 2-D viscous wave decay.

Grid (ni x nj)	4th oa compact	6th oa compact	3rd(4th) oa ENO
16 x 16	0.14×10^{-6}	0.10×10^{-7}	-
32 x 32	0.77×10^{-8}	0.15×10^{-9}	0.53×10^{-5}
64 x 64	0.47×10^{-9}	0.27×10^{-11}	0.32×10^{-6}
128 x 128	0.71×10^{-10}	0.11×10^{-12}	0.20×10^{-7}
Order(N)	4.0	6.0	4.0

4. CONCLUDING REMARKS

A higher order accurate numerical procedure has been developed for solving incompressible Navier-Stokes equations for 2D or 3D fluid flow problems.

The importance of using a consistent order of discretization in the solution of the Poisson equation for pressure is demonstrated. To guarantee a given global order of accuracy, the same compact finite-difference discretization used for the velocity derivatives should be used for the derivatives in the Poisson equation, as well as in metric terms which arise when dealing with curvilinear physical grids.

Temporal and spatial accuracy of the method is demonstrated by application to several pertinent benchmark problems.

(Manuscript received, October 17, 1997)

REFERENCES

1) S. K. Lele, Journal of Computational Physics, Vol. 103, pp. 16-42, 1992.
2) Z. Haras and S. Ta'asan, Journal of Computational Physics, Vol. 114, pp. 265-279, 1994.
3) F.Q. Hu, M.Y. Hussaini and J. Manthey, ICASE Report 94-102.
4) K. Akselvoll and P. Moin "Large Eddy Simulation of Turbulent Confined Coannular Jets and Turbulent Flow over a Backward Facing Step", Report TF-63, Department of Mechanical Engineering, Stanford University, 1995.
5) W. Rodi , J.H. Ferziger, M. Breuer and M. Pourquie, Journal of Fluids Engineering, Vol. 119, No. 2, pp. 248-262, 1997.
6) C.K.W. Tam and J.C. Webb, Vol. 103, pp. 262-281, 1993.
7) R.V. Wilson, A.O. Demuren and M. Carpenter, "Higher-Order Compact Schemes for Numerical Simulation of Incompressible Flows", ICASE Report (in preparation).
8) S.L. Lowery and W.C. Reynolds, "Numerical Simulation of a Spatially-Developing Mixing Layer," Report TF-26, Department of Mechanical Engineering, Stanford University, 1986.
9) M.H. Carpenter and C.A. Kennedy, "Fourth-Order, 2 N-Storage Runge-Kutta Schemes," NASA TM 109112, 1994.
10) S.A. Orszag, Journal of Fluid Mechanics, Vol. 49, Part 1, pp. 75-112, 1971.
11) J.T. Stuart, Journal of Fluid Mechanics, Vol. 29, Part 3, pp. 417-440, 1967.
12) A.O. Demuren and R.V. Wilson, Journal of Fluids Engineering, Vol. 116, pp. 216-220, 1994.
13) F.M. Najjar and D.K. Tafti, Physics of Fluids, Vol. 8, No. 4, pp. 1076-1088, 1996.
14) E. Weinan and C. W. Shu, ICASE Report 92-39.